Journal of Power Sources 221 (2013) 308–317

Contents lists available at SciVerse ScienceDirect

Journal of Power Sources

journal homepage: www.elsevier.com/locate/jpowsour

An integrated mathematical tool aimed at developing highly performing and cost-effective fuel cell hybrid vehicles☆

Marco Sorrentino*, Cesare Pianese, Mario Maiorino

Department of Industrial Engineering, University of Salerno, Fisciano, Salerno 84084, Italy

HIGHLIGHTS

- ► Model-based optimization of fuel cell hybrid vehicles.
- ► Versatile and online applicable energy management strategy.
- ► Optimal and specifications independent design of powertrain and control strategies.
- ► The proposed methodology aims at both energy saving and cost-effective solutions.
- ► Use of an extended database of unit mass and cost of main hybridizing devices.

ARTICLE INFO

Article history:
Received 2 May 2012
Received in revised form
30 July 2012
Accepted 1 August 2012
Available online 9 August 2012

Keywords:
PEM
Fuel cell hybrid vehicle
Modeling
Control
Design

ABSTRACT

An integrated mathematical tool is presented to simultaneously design powertrain and control strategies for PEM fuel cell hybrid vehicles. Such an activity is motivated by the positive impact of car electrification on transportation related GHG emissions, and by the potential of hydrogen as an intensive energy carrier to avoid heavy battery packs, as required for pure electric cars. Moreover, the availability of reliable and comprehensive mathematical tools is recognized as a key to develop cost effective and highly performing innovative powertrains.

A database of hybridizing devices' costs and weights is developed and exploited in conjunction with a weight model to size the powertrain as a function of degree of hybridization. In parallel, a versatile heuristic control strategy is proposed to easily adapt control rules to different powertrains. Then, both the weight model and the heuristic control strategy are embedded into an optimization procedure to determine the most convenient PEM fuel cell hybrid vehicle configuration.

The methodology is tested for a fuel cell hybrid shuttle, whose hydrogen feeding is guaranteed by a photovoltaic on-site generation system. Such a case study not only is suitable to assess the proposed optimization procedure, but also serves at indicating the most promising short-term applications of fuel cell hybrid vehicles.

1. Introduction

In the last years the increasing interest in energetic and environmental problems has given a strong impulse toward the development of alternative energy conversion devices. Since transportation systems are responsible for most of fossil fuels consumption and environmental impact, significant attention has been given to the development of alternative powertrains. Nowadays, a large variety of vehicles are considered as valid candidates to build up a sustainable mobility worldwide. In the short term scenario, hybrid electric vehicles (HEV) powered by internal combustion engine as main propulsion device surely represent the most viable solution, thanks to their mature technology and acceptable investment cost. In the medium-term scenario, plugin HEVs, which are already ready to enter the car-market today, are expected to overcome HEVs as best alternative powertrains, especially if the foreseen trends in Lithium-battery technology and costs, along with suitable adaptation of electric grids, will be met. The latter expectation will at the same time drive car makers toward massive electrification of their products, preferring series to

☆ Accepted for oral presentation (speech given on April 12 2012 by M. Sorrentino) at the Fuel Cell Science and Technology Conference (FUCE 2012), a Grove fuel cell event, held in Berlin on April 11–12.

* Corresponding author. Tel.: +39 (0)89 96 4100; fax: +39 (0)89 96 4037.
E-mail address: msorrentino@unisa.it (M. Sorrentino).

0378-7753/$ – see front matter © 2012 Elsevier B.V. All rights reserved.
http://dx.doi.org/10.1016/j.jpowsour.2012.08.001

Nomenclature

A	vehicle frontal area [m^2]
AD	annual distance [km]
aux	fuel cell system auxiliaries
B	battery
C	cost [€]
c	unit cost [€ kW^{-1}]
Cbus	conventional bus
CD	charge depleting
c_{Diesel}	cost of Diesel [€ l^{-1}]
C_E	cost of the electrolyzer [€]
C_r	rolling resistance
CS	charge sustaining
CV	conventional vehicle
C_{wat}	cost of water [€]
C_x	coefficient of drag
E_B	battery pack capacity [kW h]
E_{HT}	energy stored in the hydrogen tank [kW h]
EM	electric motor
EN	electric node
E_{PV}	electricity produced by the photovoltaic plant [kW h]
FCS	fuel cell system
FE	fuel economy [km l^{-1} or km kg^{-1}]
FiT	Feed-in Tariff [€ kW h^{-1}]
g	acceleration of gravity [m s^{-2}]
GB	gear box
HEV	hybrid electric vehicle
HFCV	hybrid fuel cell vehicle
HHV_{H_2}	hydrogen higher heating value [MJ kg^{-1}]
HT	hydrogen tank
IC	investment cost [€]
ICE	internal combustion engine
I_{chg}	battery charging current
I_{dis}	battery discharging current
M	mass [kg]
m	unit mass [kg kW^{-1}]
k_b	battery unit cost [€ kW^{-1} h^{-1}]
k_{HT}	hydrogen tank unit cost [€ kW^{-1} h^{-1}]
MC	maintenance cost for PV plant [€]
M_{Bc}	mass of a single battery cell [kg]
$\dot{m}_{H_2}$	hydrogen mass flow [kg s^{-1}]
N_{Bc}	number of battery cells
OCV	battery open circuit voltage [V]
P	power [kW]
P^*	nominal power [kW]
P^*_{Bc}	nominal power of single battery cell [kW]
PEM	proton exchange membrane
$P_{FCS,opt}$	FCS most efficient operating point [kW]
PHFCB	plugin hybrid fuel cell bus
P_{tr}	traction power [kW]
RB	rule based
R_{in}	battery internal resistance [Ohm]
SOC	battery state of charge
Stack	PEM fuel cell stack
T	vehicle transmission
TAS	total annual saving [€]
t_{end}	driving route duration [min]
v	vehicle speed [m s^{-1}]

parallel architecture to maximize battery capacity, with the final aim of extending pure electric autonomy as much as possible. Such a massive electrification not only encourages widespread diffusion of pure electric cars, especially for urban driving, but also acts as a bridge toward the introduction of hybrid fuel cell vehicles (HFCV), which are a natural evolution of series plugin HEVs as they mainly require to replace the ICE-based generator by a much more efficient fuel cell system (FCS).

The reason why HFCV success in the automotive field is considered late to arrive, despite fuel cell technology (especially PEM) has significantly matured in the last decade, is strictly related to hydrogen production, delivery and on-board storage. One solution that can reasonably be pursued in the short term is to produce hydrogen on-site via grid connected photovoltaic panels (PV), thus making the production of hydrogen economically and technically viable. This not only solves the problem of transporting hydrogen, but also promotes the technology and gives opportunities for early markets, mainly relying on currently worldwide available Feed-in-Tariffs (FiTs) associated to PV deployment for on-site electricity generation [10]. Particularly, FiTs can surely encourage the development of niche applications of HFCV powertrain, which of course are to be considered as highly strategic with respect to future establishment of such vehicular technology.

Moreover, as experienced by the automotive industry since the 1980s, both the appropriate powertrain sizing and definition of optimal control strategies have to be pursued by developing suited simulation tools, which account for the mutual interferences between all the involved variables, ranging from design to control and exogenous variables, as shown in Fig. 1. Nevertheless, while the interacting problems of optimal powertrain design [1–3] and on board energy management [4–8] of HFCVs were often dealt with separately in the literature, there is a minor contribution on their simultaneous optimization [9]. Therefore, the current study focuses on the development of an integrated computational structure aimed at supporting the HFCV powertrain design, while guaranteeing that suitable control strategies are implemented. Such an approach is herein proven suitable to yield on output powertrain design solutions that ensure the best trade-off among energy savings, proper operation of main hybridizing devices and cost effectiveness targets.

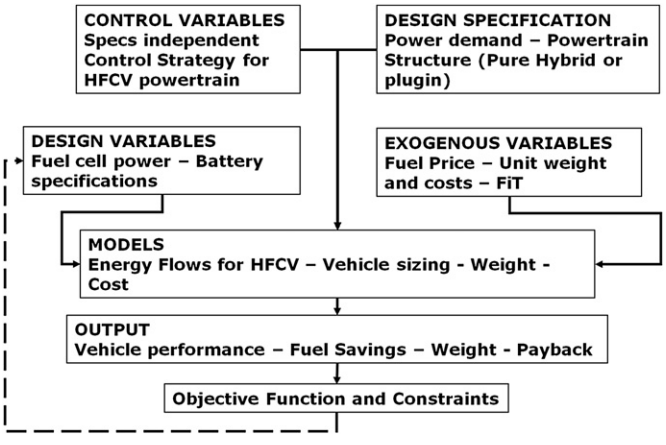

Fig. 1. Integrated mathematical tool structure.

The paper is structured as follows: firstly, the modeling approach followed to suitably treat the massive interaction among design, control, exogenous variables and constraints is presented; then, the versatile heuristic strategy developed to ensure optimal energy management be guaranteed on board, independently of powertrain configuration and component specifications, is described and discussed. Finally, a case study is developed to highlight the effectiveness of the proposed methodology.

2. Integrated mathematical tool for optimal design and on board energy management

Fig. 1 illustrates the mathematical tool concept that was conceived to enhance the development of highly performing and cost-effective HFCVs. As expected, several variable classes (e.g. design and control variables) interact with each other while simultaneously defining optimal energy management and powertrain sizing. Such interactions are suitably treated by means of an integrated modeling tool, which was developed aiming at performing optimization analyses in a wide range of all the input variables listed in Fig. 1. Such an objective may only be pursued via a modeling approach that fulfills the conflicting needs of satisfactory accuracy and acceptable computational burden, thus leading to the development of the set of sub-models described in the next sections.

The whole modeling tool yields on output significant metrics, such as fuel economy, vehicle weight and cost, which suitably account for the impact of different design specifications (e.g. passenger car or bus application) and exogenous variables (e.g. FiT) on the powertrain design optimality. The FiT influence is of particular relevance, due to its significant role into the short/medium-term deployment of emerging, highly innovative powertrains, such as HFCV [11–13].

The opportunity of evaluating the above mentioned metrics, taking into account the simultaneous effect of different variables variation, will in turn make it possible to single out powertrain designs that meet the conflicting needs of cost effectiveness and energy performance, while ensuring optimal on board management of energy flows be performed. This latter objective was achieved in this paper by developing a versatile, rule-based control strategy, conceived in such a way as to ensure that specifications-independent control strategies are selected prior to be fed as input to the integrated tool, as shown in the upper left corner of Fig. 1.

2.1. Mass model

A parametric model was set up to assess the impact of hybridization on vehicle mass. By referring to the vehicle architecture shown in Fig. 2, the mass of a HFCV can be obtained by adding the mass of major hybridizing devices to the vehicle body mass. This latter is derived from the mass of the reference conventional vehicle (CV) by subtracting the contributions due to the original gear box and ICE from the original CV mass, as follows:

$$M_{\text{body}} = M_{\text{CV}} - P^*_{\text{ICE,CV}} \cdot (m_{\text{ICE}} + m_{\text{GB}}) \tag{1}$$

Then, vehicle mass can be determined adding the hybridization devices and by imposing that the HFCV power to weight ratio (i.e. ρ_{PtW}) equals CV one, thus ensuring HFCV guarantees the same CV acceleration performance:

$$M_{\text{HFCV}} = M_{\text{body}} + P^*_{\text{FCS}} m_{\text{FCS}} + P^*_{\text{EM}} m_{\text{EM}} + M_{\text{Bc}} N_{\text{Bc}} + M_{\text{HT}} \tag{2}$$

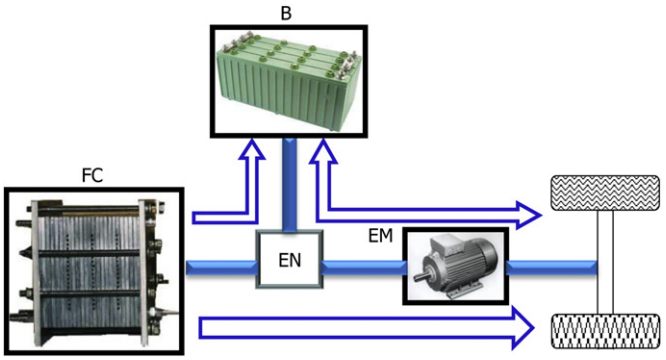

Fig. 2. Series architecture.

$$N_{\text{Bc}} = \frac{P^*_{\text{EM}} - P^*_{\text{FCS}}}{P^*_{\text{Bc}}} \tag{3}$$

$$M_{\text{HFCV}} = \frac{P^*_{\text{EM}}}{\rho_{\text{PtW}}} = \frac{P^*_{\text{EM}}}{\frac{P^*_{\text{ICE,CV}}}{M_{\text{CV}}}} \tag{4}$$

Table 1 lists the unit mass here assumed for each powertrain component.

It's worth remarking here that the nominal power of the battery's single cell (P^*_{Bc}) was assumed hereinafter constantly equal to 1.25 kW [28]; therefore, the single cell mass can be obtained as a function of either specific energy or specific power, which are univocally linked to each other as shown in Fig. 6. This is a basic point in the automatic hybrid powertrain sizing that is performed by the proposed mathematical tool.

2.2. Cost model

This section focuses on the development of a HFCV cost model, which the economical feasibility analysis discussed in Section 4 is

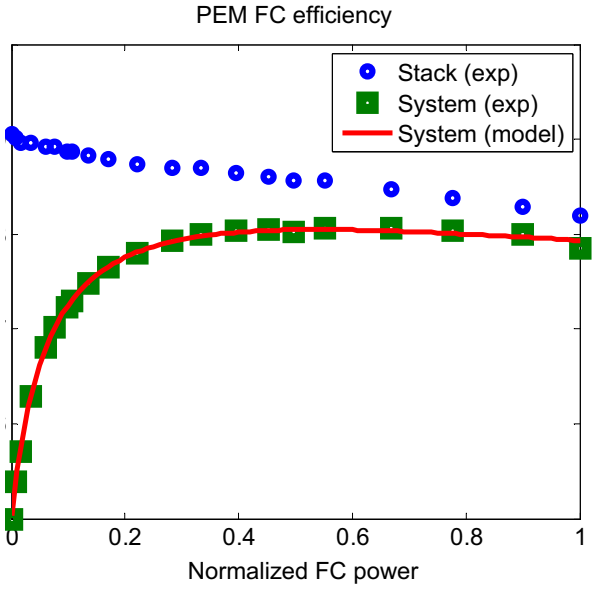

Fig. 3. FCS efficiency curves estimated from measurements performed at eProLab-UNISA.

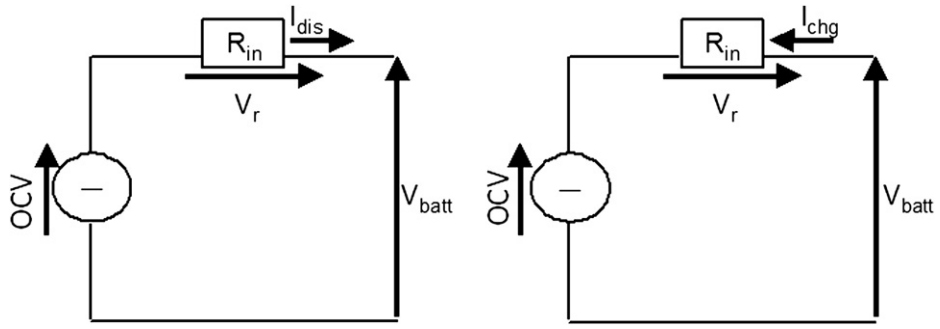

Fig. 4. Kirchoff law-based approach to battery modeling.

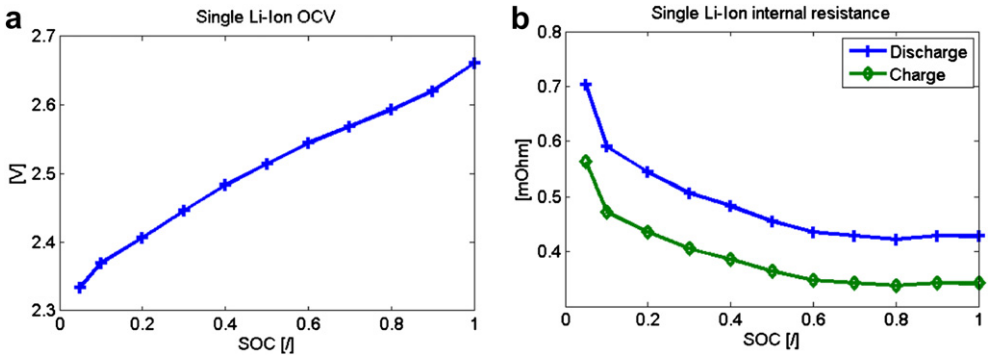

Fig. 5. (a) Single Lithium cell OCV vs. SOC; (b) single Lithium cell internal resistances vs. SOC.

based on. Such a model allows estimating the HFCV cost, which results to be greater than conventional vehicle by the amount required to hybridize the powertrain. First of all, the vehicle body cost is determined subtracting the cost of the internal combustion engine, no longer present in the HFCV, to CV global cost, as follows:

$$C_{body} = C_{CV} - c_{ICE} \cdot P^*_{ICE} \quad (5)$$

where the ICE unit cost was assumed equal to 24 € kW^{-1}. Therefore, the HFCV overall cost can be estimated taking into account the additional costs due to hybridizing devices' addition:

$$C_{HFCV} = C_{body} + c_{FCS} \cdot P^*_{FCS} + k_B \cdot E_B + c_{EM} \cdot P^*_{EM} + k_{HT} \cdot E_{HT} \quad (6)$$

where the EM unit cost (including the inverter) equals 16.8 € kW^{-1} [20,21]. On the other hand, the unit cost of fuel cells, hydrogen tank and batteries is closely linked to production volumes. For this reason, three cost scenarios were assumed (see Table 2) for the main hybridizing devices, aiming at correctly estimating future trends in HFCV economical feasibility. Particularly, the dependence of PEM FCS cost on production volume was derived from Ref. [22], while the battery cost trend proposed in Table 2 was adapted from the Lithium-battery price forecast proposed in Ref. [23]. Instead, the volume 1 cost of the hydrogen tank is assumed equal to the average cost reported in Ref. [24], whereas the costs associated to volume 2 and 3 were estimated assuming a proportional relationship with FCS cost trend. It is worth mentioning here that the hydrogen tank cost assumed for volume 3 well agrees with the value given in Ref. [25].

Table 1
Components unit mass [12–19].

Internal combustion engine [kg kW^{-1}]	2
Gear box [kg kW^{-1}]	0.478
Electric motor (including inverter) [kg kW^{-1}]	1
PEM Fuel cell system [kg kW^{-1}]	3.70
Hydrogen tank [kW h kg^{-1}]	1.9

2.3. Longitudinal vehicle model

Fuel economies in this paper are evaluated by means of a backward longitudinal vehicle model developed in Matlab® environment, whose basic equations are presented below.

Road load is estimated as:

$$P_{tr} = M_{HFCV} \cdot g \cdot v \cdot [C_r \cos(\alpha) + \sin(\alpha)] + 0.5\rho C_x A v^3 + M_{eff} \frac{dv}{dt} v \quad (7)$$

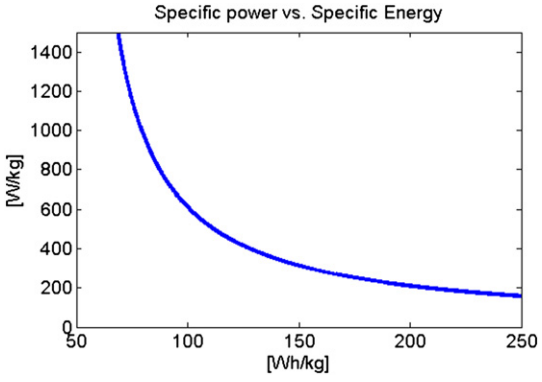

Fig. 6. Relationship between Li-ion battery specific power and specific energy.

Table 2
Cost trends assumed for the main HFCV hybridizing devices.

Annual production volumes	Volume 1 (1000 units)	Volume 2 (100,000 units)	Volume 3 (500,000 units)
Fuel cell system [€ kW^{-1}]	175	54	39
Battery [€ kW h^{-1}]	1500	1000	500
Hydrogen tank [€ kW h^{-1}]	81	25	18

where α and ρ are the road grade and air density, respectively, while M_{eff} equals 1.1 M_{HFCV} to suitably account for rotational inertia. For non negative P_{tr} values, the mechanical power to be supplied by the EM is (see Fig. 2):

$$P_{EM} = \frac{P_{tr}}{\eta_T} \quad \text{if} \quad P_{tr} \geq 0 \tag{8}$$

P_{EM} can also be expressed as a function of FCS and battery power, as follows:

$$P_{EM} = \eta_{EM}(P_{FCS}\eta_{FCS} + P_B) \quad \text{if} \quad P_{tr} \geq 0 \tag{9}$$

where the η variables correspond to efficiency terms. On the other hand, when $P_{tr} < 0$, the regenerative braking mode is active, resulting in the following expression for the electrical energy delivered by the EM:

$$P_{EM} = P_{tr}\eta_T\eta_{EM} \quad \text{if} \quad P_{tr} < 0 \tag{10}$$

During regenerative braking, battery can be charged by FCS also, thus the following equation holds for negative P_{tr} values:

$$P_B = P_{EM} - P_{FCS}\eta_{FCS} \quad \text{if} \quad P_{tr} < 0 \tag{11}$$

It is worth remarking here that EM efficiency is computed by means of normalized maps derived from the model library proposed in Ref. [26], whereas FCS and battery efficiencies are estimated via the respective sub-models presented in Sections 2.4 and 2.5.

2.4. Modeling of fuel cell system efficiency

In this paper, a proton exchange membrane fuel cell was considered. In order to estimate hydrogen fuel economy dependency on main HFCV design and control variables, a normalized efficiency map was inferred by curve fitting the experimental data acquired at the PEM FC test bench available at the Energy and Propulsion Laboratory – University of Salerno (eProLab – UNISA). Particularly, both gross FC stack power and auxiliary power adsorption were measured to calculate net FCS efficiency, as follows:

$$\eta_{FCS} = \frac{P_{stack} - P_{aux}}{\dot{m}_{H_2}\mathrm{HHV}_{H_2}} \tag{12}$$

Then, the experimental FCS efficiency points were curve fitted by the following rational polynomial function:

$$\hat{\eta}_{FCS} = \frac{p_1 P_{FCS} + p_2}{q_1 P_{FCS}^2 + q_2 P_{FCS} + q3} \tag{13}$$

Fig. 3 illustrates the comparison between experimental and modeled efficiency values,[1] highlighting the accuracy achieved by the model expressed by Eq. (11). It is also worth pointing out the good qualitative agreement between the FCS efficiency curve acquired at UNISA PEM[2] test bench and previously published curves [9,27]. The values estimated via Eq. (13) are hereinafter used to evaluate the amount of H_2 consumed by HFCVs by means of Eq. (12).

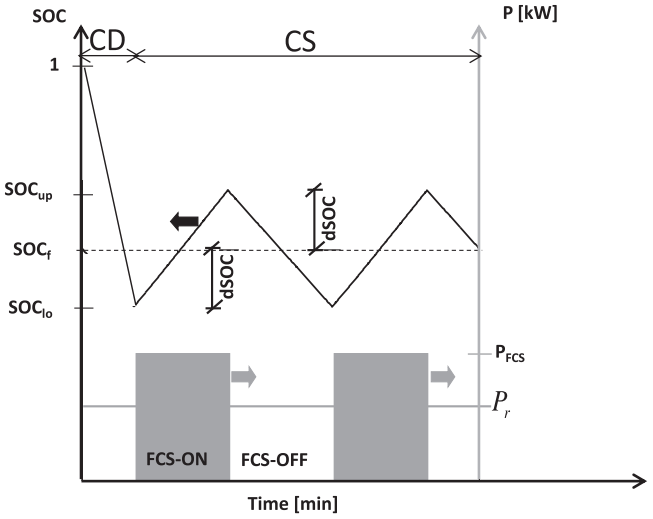

Fig. 7. Qualitative description of thermostatic management for a HFCV.

2.5. Battery model

The battery pack model estimates battery state of charge (SOC) and current as a function of the actual electric power (i.e. positive for discharge and negative for charge). The actual current is computed starting from the electrical power, by applying the Kirchoff's law to the equivalent circuit shown in Fig. 4. The dependence of main equivalent circuit parameters (i.e. OCV and R_{in}) on SOC for Lithium battery technology was modeled adapting the experimental data provided in Refs. [3] and [28]. Such nonlinear dependencies are illustrated in Fig. 5(a) and (b), respectively. Particularly, the latter figure provides the R_{in} values to be exploited in the Kirchoff law-based calculation of single cell voltage, as shown in Fig. 4.

In order to account for the impact of battery features (i.e. high power or high energy type) on HFCV powertrain performance and cost effectiveness, a further literature analysis [28,29] was carried out to infer the relationship between battery specific power and specific energy, resulting in the inverse correlation shown in Fig. 6. Such an inverse correlation, when coupled with both nominal FCS power and nominal battery's single cell power, allows precise estimation of the whole battery pack mass as a function of either specific energy or specific power.

3. Rule-based energy management of series hybrid fuel cell vehicles

The availability on HFCVs of both an electric generator (i.e. the fuel cell system) and a battery pack makes it possible to operate HFCVs in plugin mode, as shown in Fig. 7. At the beginning of the driving route, charge depleting (CD) mode is active, thus the battery capacity is firstly exploited to run the HFCV powertrain as a pure electric vehicle [30]. Afterward, once the minimum state of charge SOC_f has been reached, the plugin control strategy switches to the

[1] Both experimental and model values were omitted in Fig. 3 for confidentiality reasons.

[2] www.eprolab.unisa.it.

charge-sustaining (CS) task (see Fig. 7), through which the targeted final state of charge SOC_f is reached at the end of the cycle. Since HFCV configuration necessarily corresponds to the series architecture (see Fig. 1), the use of a simple thermostatic strategy is suitable to accomplish the CS control objective [31]. Thermostatic CS control of series hybrid vehicles was actually proven to be highly effective as compared to ideal fuel economies achievable using a-priori based dynamic programming optimization techniques [32].

Fig. 7 indicates that the thermostatic control strategy is adopted as soon as the CD phase expires, i.e. when battery state of charge decreases from fully charge conditions (SOC = 1) down to SOC_f. The battery is initially further depleted until SOC becomes lower than a given threshold, set to $SOC_{lo} = SOC_f - dSOC$. Afterward FCS is turned on at the assigned power level and switches off when the upper threshold $SOC_{up} = SOC_f + dSOC$ is reached. The procedure is repeated until the end of the driving cycle, thus ensuring charge-sustaining operation of the battery pack over the entire CS phase be achieved. The simple thermostatic strategy shown in Fig. 7 can be further improved by optimizing the parameters P_{FCS} and dSOC in such a way as to well adapt on board energy management to different driving conditions and powertrain configurations. The following section describes in detail the methodology developed to optimize such parameters.

3.1. Rule-based thermostatic management of HFCVs in charge sustaining operation

The optimal values of P_{FCS} and dSOC are estimated online as a function of current traction power demand, as follows:

$$P_{FCS} = f(\overline{P}_{tr}) \tag{14}$$

$$dSOC = g(\overline{P}_{tr}) \tag{15}$$

where the functions f and g correspond to look-up tables developed offline extending the procedure proposed in Refs [32] and [33] to series HFCV. Such a procedure aims at determining optimal f and g functions (i.e. Eqs. (14) and (15)) by solving the following minimization problem over an extended range of average traction power demand ($\overline{P}_{tr}$):

$$\min_{P_{FCS},\Delta t_{FC-OFF}} \int \dot{m}_{H_2}(P_{FCS}, \Delta t_{FCS-OFF})dt \tag{16}$$

subject to the constraint:

$$SOC(end) = SOC_f \tag{17}$$

Solving the above minimization problem corresponds to identifying the best engine intermittency (i.e. $\Delta t_{FCS\text{-}OFF}$, which is the time during which FCS is kept off) and power level at which the FCS should be operated for a given traction power demand over a specified time-horizon, here set to $t_h = 10$ min (see Fig. 8).

While the function f (i.e. Eq. (14)) is directly determined by solving the above described minimization problem (i.e. Eqs. (16) and (17)), the g relationship among dSOC and average traction power demand is determined as shown in Fig. 8, where the optimal SOC trajectory is depicted: SOC initially decreases as the FCS is imposed to be initially off; then, due to FCS switching-on, SOC trend is inverted allowing to satisfy the constraint expressed by Eq. (17). The halved difference between SOC_f and SOC_{min} (see Fig. 8) is then used to evaluate the SOC excursion (i.e. dSOC) to be adopted in the rule-based control strategy. Of course, effective on-line implementation of both rules (i.e. Eqs. (14) and (15)) entails estimating average traction power demand. Particularly, the latter variable can

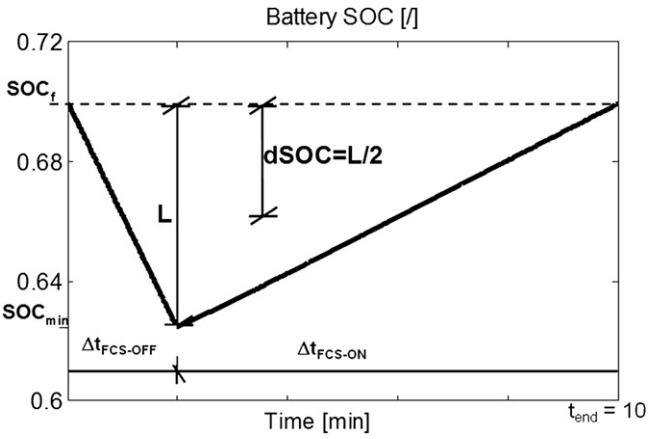

Fig. 8. dSOC indirect determination from the optimal SOC trajectory addressed by the solved minimization problem (see Eqs. (16) and (17)) for an assigned $\overline{P}_{tr}$ value.

be updated every t_h time horizon by means of either an a-priori (i.e. Eq. (18)) or an a-posteriori (i.e. Eq. (19)) method:

$$\overline{P}_{tr}(t)\big|_{t_i<t<t_i+t_h} = \frac{1}{t_h}\int_{t_i}^{t_i+t_h} P_{tr}(t)dt \tag{18}$$

$$\overline{P}_{tr}(t)\big|_{t_i<t<t_i+t_{h,i-1}} = \frac{1}{t_{h,i-1}}\int_{t_i-t_{h,i-1}}^{t_i} P_{tr}(t)dt \tag{19}$$

where i is an integer varying in the range $[0 \div (t_{end}/t_h)]$. Of course the a-priori strategy becomes suitable for on board application once coupled either to GPS information or model-based forecasting of average traction power demand.

Figs. 9 and 10 explain the variation of each heuristic rule (see Eqs. (14) and (15)). The analysis of both figures confirms the conclusions previously drawn by the authors on the intrinsic features of the proposed rule-based (RB) control strategy for series hybrid architectures [33]. In the current paper, the algorithm was further refined by normalizing both rules (i.e. Eqs. (14) and (15)), thus making them sufficiently versatile to be successfully deployed

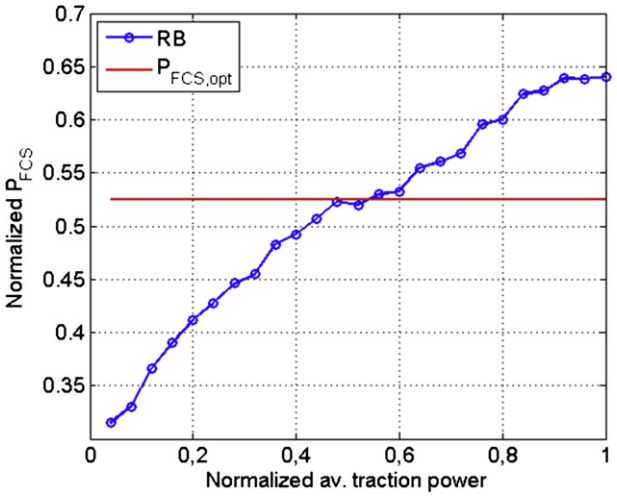

Fig. 9. Variation of optimal P_{FCS} (i.e. RB curve) as function of average traction power – (i.e. Eq. (14)).

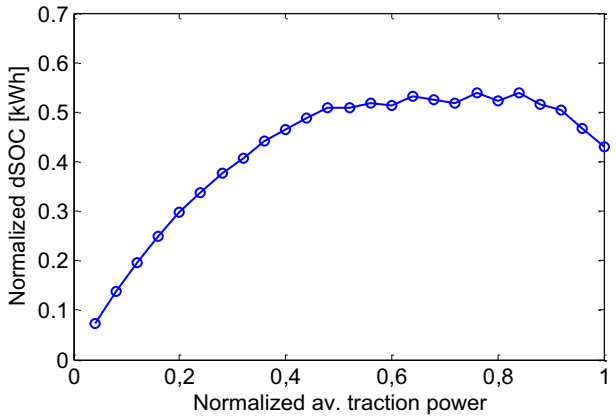

Fig. 10. Variation of optimal dSOC (i.e. RB curve) as function of average traction power – (i.e. Eq. (15)).

over a wide range of HFCV designs and applications. Particularly, both in Figs. 9 and 10, the abscissa is normalized. The effective input values of the f and g look-up tables (i.e. Eqs. (14) and (15)) are obtained multiplying such abscissa by P^*_{FCS}. In such a way, it is possible to account for the fact that the higher the value of P^*_{FCS}, the higher will be the value of optimal P_{FCS}, as shown in Fig. 3.

Regarding the ordinates of Figs. 9 and 10, the de-normalization of the rule expressed by Eq. (14) is straightforward, in that its output only needs to be multiplied by P^*_{FCS} to estimate the best power level at which the FCS should be operated. On the other hand, it is worth providing further details on how the rule expressed by Eq. (15) is obtained: for a given battery pack design, the ordinates of Fig. 10, expressed in kW h, are divided by the overall battery capacity, also expressed in kW h. This way, the rule illustrated in Fig. 10 yields higher dSOC values for smaller battery packs and vice versa, as expected.

3.2. Verification of RB strategy energy performance

As mentioned above, the reliability of thermostatic energy management for series hybrid vehicles was already tested against both dynamic programming and genetic algorithm off-line optimization [32,33]. In this section, a comparative analysis is performed to highlight the effectiveness of the RB strategy described in the previous section to further increase energy benefits associated to fuel cell hybridization of vehicles as compared to simple

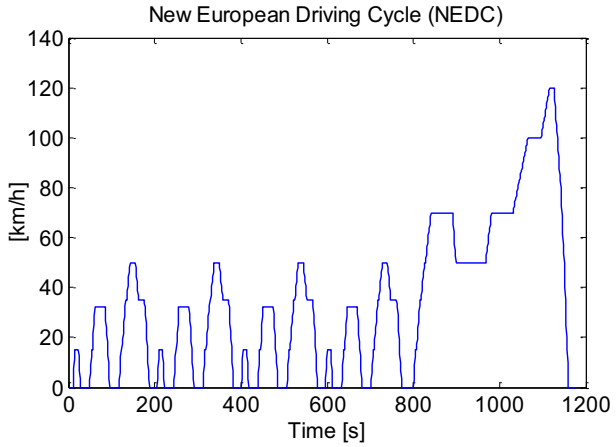

Fig. 11. New European driving cycle.

Table 3
Conventional passenger car specifications.

Length [mm]	4450
Width [mm]	1770
Height [mm]	1550
ICE power [kW]	75
Mass [kg]	1300
Coefficient of drag [/]	0.33
Coefficient of rolling friction [/]	0.01
Rolling radius [mm]	500

thermostatic management. The longitudinal vehicle model described in Section 2.3 was applied to a typical passenger car (see specifications in Table 3), which was considered for hybridization with fuel cells. Several HFCV configurations were designed applying the models developed in Section 2, assuming that: i) P^*_{FCS} varies in the range 20–60 kW; ii) battery specific energy is constantly equal to 215 W h kg^{-1}; iii) the hydrogen tank mass and energy (see Eqs. (2) and (6)) guarantee up to 400 km autonomy. Fig. 12 shows the hydrogen fuel economies simulated for the above set of HFCVs on the new European driving cycle (see Fig. 11). The comparative analysis highlights how the RB energy management outperforms simple thermostatic management, whose corresponding values were simulated assuming P_{FCS} and dSOC be constantly equal to $P_{FCS,opt}$ and 0.01, respectively. The benefits are particularly evident in case a-priori estimation of RB strategy input (i.e. average traction power) is performed, thus indicating the need for an on board predictor of future average power required at vehicle wheels. The results illustrated in Fig. 12 well agree with similar analyses available on the public domain [9], thus demonstrating the suitability of the proposed RB strategy to single out the most energy saving HFCV design (i.e. corresponding to $P^*_{FCS} = 40$ kW) once embedded into an integrated mathematical tool as the one proposed in this paper. It is worth remarking here that the proposed RB management strategy does not need to be optimized as a function of powertrain degree of hybridization, thus highlighting once again its contributing value with respect to the methodology previously developed by Kim and Peng [9].

Fig. 13 shows the P_{FCS} trajectory simulated for the most energy saving solution, both when enabling RB and simple thermostatic strategy. As expected, and as more clearly highlighted in the close window shown in Fig. 13(b), the RB strategy allows avoiding battery overcharging during low power demand phases, thus resulting in

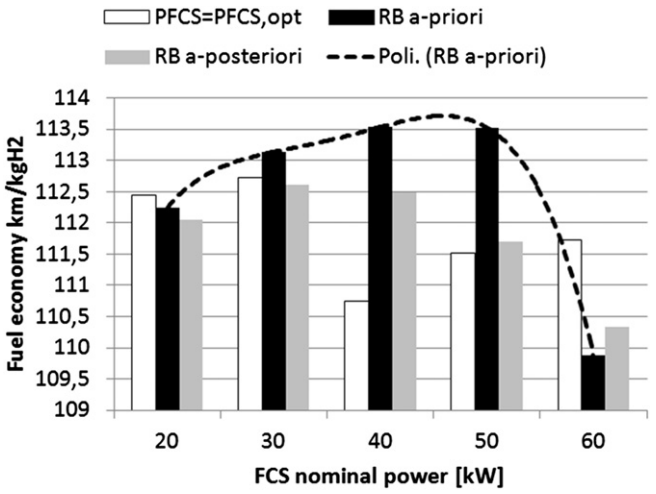

Fig. 12. Comparison of fuel economies simulated with RB and simple thermostatic energy management.

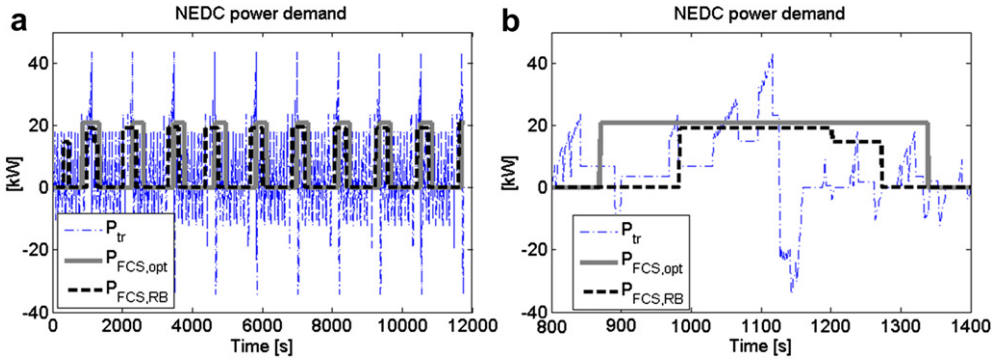

Fig. 13. (a) Comparison of simulated fuel cell power trajectories for the best fuel economy powertrain (i.e. corresponding to $P^*_{FCS} = 40$ kW, as shown in Fig. 12). (b) Close window of (a).

Table 4
Characteristics of the conventional Diesel bus.

Length [mm]	9420
Width [mm]	2330
Height [mm]	2885
Power [kW]	160
Mass [kg]	14,655
Coefficient of drag [/]	0.5
Coefficient of rolling friction [/]	0.012
Rolling radius [mm]	500
Diesel fuel economy [km l^{-1}]	2.1

a more efficient use of the battery pack. Moreover, Fig. 13(a) indicates how the RB strategy forces the FCS to provide boost power during peak power demand, thus maximizing direct flow of energy from FCS to the wheels, which in turn reduces charging/discharging dissipations associated to excessive energy storage into the battery pack.

4. Case study

The case study focuses on a real world potential early market for HFCV, namely the development of a plugin hybrid fuel cell bus (PHFCB) to be used in place of the conventional bus (Cbus, see specifications in Table 4) that is currently used as a shuttle at UNISA campus. Hydrogen feeding and battery recharging are guaranteed by an on-site PV generation system. Such a solution allows, on one hand, to deeply exploit FiT associated to photovoltaic energy generation and, on the other, to produce clean energy and thus develop a vehicle with no environmental impact. Table 5 summarizes the main features of the case study. Furthermore, the latter table specifies the value of several variables introduced in the following Eqs. (20)–(22).

In order to assess the economic feasibility of replacing the existing bus by a fuel cell vehicle, a pay-back analysis was performed. In this analysis the total investment is considered equal to the difference between the new PHFCB and the current conventional bus cost, which is then added to the photovoltaic plant and electrolyzer cost:

$$IC = C_{PHFCB} - C_{Cbus} + c_{PV} \cdot P^*_{PV} + C_E \quad (20)$$

It is worth pointing out here that both unit cost and nominal power of photovoltaic plant [35] and electrolyzer [36] depend on the PHFCB characteristics and, in turn, on its energetic performance (i.e. hydrogen fuel economy FE_{H2} [km kg^{-1}]), to be simulated as a function of powertrain specifications by means of the flexible mathematical tool presented and discussed in the previous sections. Particularly, the nominal PV power to be installed to guarantee pure photovoltaic hydrogen generation is computed as follows:

$$P^*_{PV}[kW] = \left(\frac{AD}{FE_{H_2}} \cdot \frac{HHV_{H_2} \cdot 10^{-3} \cdot 3600^{-1}}{\eta_E} + E_{PI} \right) \cdot \frac{1}{E_{PV}/P_{PV}} \quad (21)$$

where h_E and E_{PV} $P_{PV}{}^{-1}$ are the electrolyzer efficiency and the PV energy [kW h] per peak power [kW], respectively, while E_{PI} is the annual electrical energy consumed to compensate for plugin operation of the vehicle (i.e. to recharge the battery at the end of the day to increase SOC back to fully charge condition). It is worth remarking here that the value assumed for η_E in this work (i.e. 0.63 and 0.53 if higher or lower H_2 heating value is assumed, respectively [36]) is safe enough to be representative of the entire hydrogen production chain via alkaline electrolysis, including the energy spent for pressurization [37]. Eq. (21) also highlights that the only cost associated to the electricity required for hydrogen production corresponds to PV investment cost.

Table 5
Characteristics of the case study.

Daily distance [km day^{-1}]	156.7
Working days [/]	238
Annual distance [km $year^{-1}$]	37,295
Cost of Diesel fuel [€ l^{-1}]	1.80
Cost of water [€ m^{-3}]	0.75
Cost of PV panels [€ kW^{-1}]	3270
FiT[a] [€ kW h^{-1}]	0.233
PV energy per peak power [kW h kW^{-1}]	1300

[a] The assumed value corresponds to 2011 Italian FiT for PV diffusion enhancement [34].

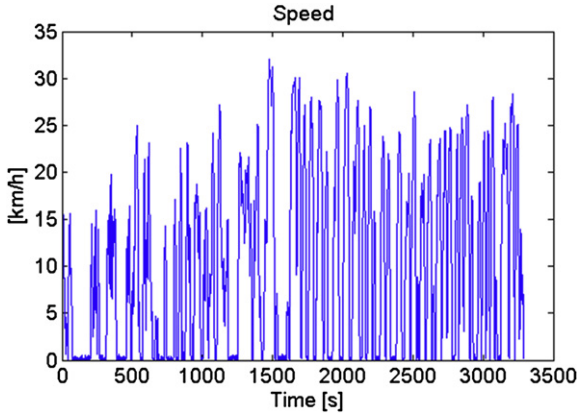

Fig. 14. Reduced speed London bus cycle.

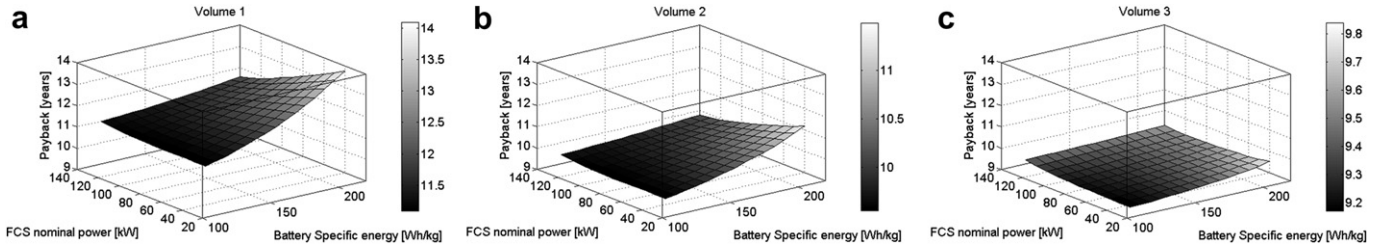

Fig. 15. Parametric analysis outcomes: (a) volume 1; (b) volume 2; (c) volume 3.

Table 6
Simulated performance for the best case shown in Fig. 15 (i.e. nominal fuel cell system power = 30 kW, battery specific energy=110 kW h).

Mass [kg]	15,571
FCS nominal power [kW]	30
Battery pack capacity [kW h]	28.4
Number of battery cells [/]	106
EM nominal power [kW]	161.5
Hydrogen fuel economy in CS phase [km kg^{-1}]	20.72
Diesel equivalent fuel economy [km l^{-1}]	4.21
Energy consumption in CD phase [W h km^{-1}]	745

Regarding electrolyzer cost, in this work it is evaluated as a function of daily hydrogen production, by means of the relationship proposed in Ref. [36]. It is also worth mentioning that such relationship, which holds valid as it is for the volume 1 scenario (see Table 2), is adapted to production volumes 2 and 3 by proportionally scaling its output with respect to FCS cost reduction.

The total annual savings is instead related to the saved Diesel consumption and FiT, to which however the cost of water needed for electrolysis and the PV annual maintenance cost (here set equal to 1% of entire PV plant cost) must be subtracted:

$$\mathrm{TAS} = \left(\frac{\mathrm{AD}}{\mathrm{FE}_{\mathrm{Cbus}}}\right)\cdot c_{\mathrm{Diesel}} + E_{\mathrm{PV}}\cdot \mathrm{FiT} - C_{\mathrm{wat}} - \mathrm{MC} \tag{22}$$

The payback can then be evaluated as:

$$\mathrm{Payback} = \frac{\mathrm{IC}}{\mathrm{TAS}} \tag{23}$$

The pay-back analysis was applied to the three production volumes shown in Table 2, thus accounting for the impact of market penetration of hybridizing devices on PHFCB comprehensive cost. In addition, for each production volume a parametric analysis was performed to evaluate payback variation as a function of nominal fuel cell system power and battery specific energy, in the ranges [30, 130] kW and [110, 220] kW h, respectively. Such an analysis was conducted simulating the PHFCB on a real world bus driving schedule, namely the London bus cycle (see Fig. 14). In this case, the mass and cost models (see Sections 2.1 And 2.2) were deployed assuming that hydrogen tank size ensures up to 150 km autonomy, which is consistent with the case study characteristics (see Table 5) and with the fact that PHFCB is run as a plugin vehicle. Battery mass was computed by suitably coupling Eqs. (2)–(4) to the information on battery specific power retrievable from Fig. 6. It is also worth remarking here that the versatile features of the RB management strategy presented in Section 3.1 were exploited by adapting the rules described in Figs. 9 and 10 to the varying values of FCS nominal power and battery specific energy considered in the parametric analysis.

Fig. 15 shows the results of the above described analysis. As expected, projected reduction in hybridizing devices cost will enhance economic feasibility of the proposed solution. More interesting to note is the fact that a range-extender like powertrain design (i.e. low P^{*}_{FCS}) emerges as the best compromise between energetic performance and cost effectiveness (see Table 6). There are two main justifications of such a result. First of all, buses do not suffer so significantly from hybridization mass increase, thus resulting in negligible differences in energetic performance when switching from one degree of hybridization to another (i.e. by either reducing or increasing nominal FCS power). Moreover, reducing nominal FCS power results in higher battery nominal power (see Section 2.1), which in turn causes battery storage capacity to increase without needing high energy density (see Fig. 6). This way, plugin effect is better exploited as compared to high P^{*}_{FCS} solutions (see Fig. 15), without requiring such a high investment cost for both battery pack and fuel cell system. In this context, the availability of a previously optimized control strategy (see Section 3), which is suitable to be embedded within the integrated mathematical tool proposed in this paper, was shown to be effective in ensuring optimization analyses be conducted without over-simplifying

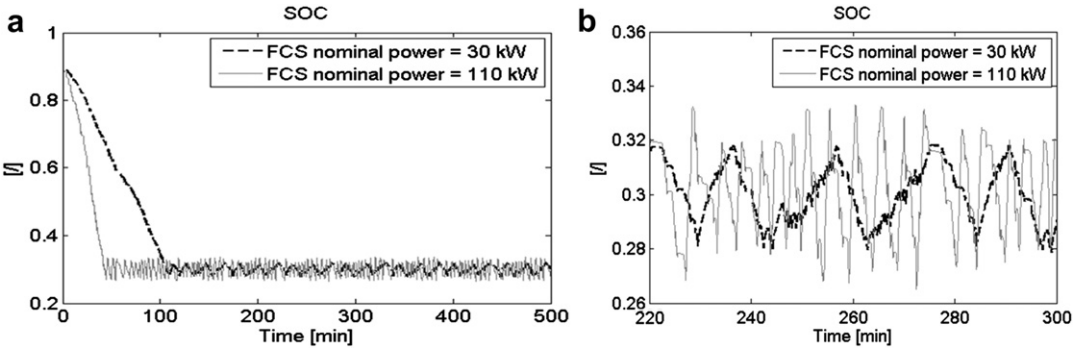

Fig. 16. (a) Comparison of simulated SOC trajectories. (b) Close window of (a).

hypotheses. Usually, one common over-simplification relates to how is accounted for the dependence of powertrain energetic performance on design specifications and vehicle application (i.e. prevailing urban use of the bus-shuttle, which the case study focuses on).

Finally, the selection of a range-extender like PHFCB design appears satisfactory even from a battery lifetime point of view, as it emerges from Fig. 16, where the SOC trajectories simulated for both the best and the $P^*_{FCS} = 110$ kW solutions are compared. Particularly, the SOC trajectory associated to $P^*_{FCS} = 110$ kW exhibits a higher frequency oscillation around the targeted SOC_f, which in turn might lead to higher number of equivalent DOD with respect to $P^*_{FCS} = 30$ kW.

5. Conclusions

An integrated mathematical tool was conceived to simultaneously optimize powertrain sizing in hybrid fuel cell vehicles and their control strategies. The models were developed aiming at finding the best compromise between conflicting needs, such as accuracy and computational burden, thus making the proposed methodology suitable to run extended optimal design oriented analyses.

Moreover, the integration of the modeling tool with a versatile heuristic strategy was proven to be effective to guarantee high performance be achieved independently of vehicle typology, specifications and destination of use.

A case study was proposed to show the potential of FC hybridization provided that suitable optimal design and energy management are guaranteed. The results obtained for a bus shuttle are in line with what was previously addressed and tested by other researchers active in the field [38], thus confirming the potential of the proposed methodology.

Acknowledgments

The research presented is partially funded by Campania Regional Government (D.R. n. 134, 11/03/2010 – L.R. 5/02). Mr. Gianpaolo Noschese and Mr. Raffaele Petrone of Energy and Propulsion Laboratory at University of Salerno are gratefully acknowledged for the experimental data provided.

References

[1] K. Kobayashi, M. Miyatake M, Analysis of optimum unit sizing of a hybrid vehicle composed of fuel cell and electric double layer capacitor by dynamic programming, in: Proceedings of the 2010 International Conference on Electrical Machines and Systems, ICEMS2010, art. no. 5663856, pp. 2031–2035.
[2] X. Liu, D. Diallo, C. Marchand, International Journal of Automotive Technology 12 (2011) 433–441.
[3] J. Han, P.Y. Papalambros, Journal of Fuel Cell Science and Technology 7 (2010) 0210201–0210209.
[4] P. Rodatz, G. Paganelli, A. Sciarretta, L. Guzzella, Control Engineering Practice 13 (2005) 41–53.
[5] G. Paganelli, Y. Guezennec, G. Rizzoni, Optimizing control strategy for hybrid fuel cell vehicle, in: Proceedings of SAE 2002 World Congress & Exhibition, March 2002, Detroit, MI, USA.
[6] I. Arsie, A. Di Domenico, C. Pianese, M. Sorrentino, Journal of Fuel Cell Science and Technology 4 (2007) 261–271.
[7] A. Fadel, B. Zhou, Journal of Power Sources 196 (2011) 3271–3279.
[8] P. Bubna, D. Brunner, S.G. Advani, A.K. Prasad, Journal of Power Sources 195 (2010) 6699–6708.
[9] M.J. Kim, H. Peng, Journal of Power Sources 165 (2007) 819–832.
[10] J.M. Ogden, M. Steinbugler, T. Kreutz, Hydrogen energy systems studies, in: Proceedings of the 1998 U.S. DOE Hydrogen Program Review, NREL/CP-570-25315.
[11] S.G. Chalk, P.G. Patila, S.R. Venkateswaranb, Journal of Power Sources 61 (1996) 7–13.
[12] C.E. Thomas, B.D. James, F.D. Lomax Jr., International Journal of Hydrogen Energy 23 (1998) 949–966.
[13] H. Zhou, F. Wei, S. Liqing, Journal of Asian Electric Vehicles 2 (2004) 531–534.
[14] http://www.abb.com/ProductGuide/Alphabetical.aspx.
[15] http://www.fimea.it/produzione/trazione/n60.htm.
[16] http://www.iliofos.gr/ILIOFOS%20C.O.%20Us/Pdf's/PP75%20Spec%20Sheet%207.14.10.pdf.
[17] http://www.gielow.org/PowerPhase100.pdf.
[18] G. Dawei, J. Zhenhua, L. Qingchun, Journal of Power Sources 185 (2008) 311–317.
[19] M. Klell, in: M. Hirscher (Ed.), Handbook of Hydrogen Storage. New Materials for Future Energy Storage, Wiley-VCH Verlag, Weinheim, 2010, pp. 32–35.
[20] I. Arsie, M. Marotta, C. Pianese, G. Rizzo, M. Sorrentino, Optimal design of a hybrid electric car with solar cells, in: Proceedings of 1st AUTOCOM Workshop on Preventive and Active Safety Systems for Road Vehicles, 19–20 September 2005, Istanbul, Turkey.
[21] http://www1.eere.energy.gov/vehiclesandfuels/pdfs/mypp/1_prog_over.pdf.
[22] B.D. James, J.A. Kalinoski, Mass Production Cost Estimation for Direct H_2 PEM Fuel Cell Systems for Automotive Applications: 2008 Update (March 26, 2009). Available at: http://www1.eere.energy.gov/hydrogenandfuelcells/pdfs/mass_production_cost_estimation_report.pdf. v.30.2021.052209.
[23] http://www.greencarcongress.com/2012/03/pike-20120312.html.
[24] F. Di Mario, Idrogeno come vettore energetico per un futuro sostenibile, ENEA, Cagliari, 2004, Available at: http://www.cagliari.cgil.it/vecchiosito/convegno%20energia%20atti/relazione%20enea.pdf (in Italian).
[25] T. Hua, R. Ahluwalia, J.-K. Peng, M. Kromer, S. Lasher, Technical Assessment of Compressed Hydrogen. Storage Tank Systems for Automotive Applications, Argonne National Laboratory, 2010, Available at: http://www.hydrogen.energy.gov/pdfs/10004_fuel_cell_cost.pdf.
[26] A. Rousseau, P. Sharer, R. Ahluwalia, Energy storage requirements for fuel cell vehicles, in: SAE Paper 2004-01-1302, Proceedings of the SAE 2004 World Congress & Exhibition, March 2004, Detroit, MI, USA.
[27] I. Arsie, A. Di Domenico, L. Pappalardo, C. Pianese, M. Sorrentino, Steady-state analysis and energetic comparison of air compressors for PEM fuel cell systems, in: Proceedings of the 4th International Conference on Fuel Cell Science, Engineering and Technology, 19–21 June 2006, Irvine, CA, USA.
[28] P. Nelson, K. Amine, A. Rousseau, Advanced Lithium-ion Batteries for Plug-in Hybrid-electric Vehicles. Available at: www.transportation.anl.gov/pdfs/HV/461.pdf.
[29] IEA, Technology Roadmaps: Electric and Plug-in Hybrid Electric Vehicles. Available at: http://www.iea.org/papers/2011/EV_PHEV_Roadmap.pdf.
[30] P. Tulpule, V. Marano, G. Rizzoni, International Journal of Electric and Hybrid Vehicles 2 (2010) 329–350.
[31] S. Barsali, C. Miulli, A. Possenti, IEEE Transactions on Energy Conversion 19 (2004) 187–195.
[32] Sorrentino M, Rizzo G, Vasca F. An energetic comparison for hybrid vehicles ranging from low to high degree of hybridization, in: SAE Paper 2011-24-0086, Proceedings of the 10th International Conference on Engines & Vehicles, 11–15 September 2011, Capri, Italy.
[33] M. Sorrentino, G. Rizzo, I. Arsie, Control Engineering Practice 19 (2011) 1433–1441.
[34] Autorità per l'energia elettrica e il gas. Available at: http://www.autorita.energia.it/it/index.htm (in Italian).
[35] www.solarbuzz.com.
[36] G. Saur, Electrolyzer Capital Cost Study. Wind-To-Hydrogen Project: NREL/TP-550-44103 (December 2008). Available at: http://www.osti.gov/bridge.
[37] S. Ibrahim, J. Poindexter, Alkaline Electrolysis. 2006 DOE H_2 Program Review. Available at: http://www.hydrogen.energy.gov/pdfs/review06/pd_9_ibrahim.pdf.
[38] http://www.fuelcells.org/info/charts/buses.pdf.